Redox-Dependent Isomerization of Organometallic Ru^{II}/Ru^{III} Compounds Containing the Hydrotris(methimazolyl)borate Ligand: An Electrochemical Square Scheme Mechanism

Seah Ling Kuan, Weng Kee Leong, and Lai Yoong Goh*

Department of Chemistry, National University of Singapore, Kent Ridge, Singapore 117543

Richard D. Webster*

Research School of Chemistry, Australian National University, Canberra, Australian Capital Territory 0200, Australia

Received May 31, 2005

[$Cp^*Ru^{III}\{HB(mt)_3\}$]X (**1A**(X); X = Cl, PF_6) and [$Cp^*Ru^{II}\{HB(mt)_3\}$] (**2A**) ($Cp^* = \eta^5$-C_5Me_5, mt = *N*-methyl-2-mercaptoimidazol-1-yl) were synthesized by the reactions of K[$HB(mt)_3$] with [$Cp^*Ru^{III}Cl_2]_2$ and [$Cp^*Ru^{II}(OMe)]_2$, respectively. **1A** and **2A** exist in the solid state in κ^3-S,S′,S″ coordination, so that the sulfur atom in each mt group coordinates to the central Ru ion, producing the normal tripodal geometry of the [$HB(mt)_3$] ligand. However, both compounds undergo an isomerization reaction in solution, where the sulfur on one mt group is displaced in favor of coordination to the hydrogen bonded to the boron (an agostic B−H−Ru interaction), resulting in κ^3-H,S,S′ coordination about the Ru (κ^3-H,S,S′ forms of [$Cp^*Ru^{III}\{HB(mt)_3\}$] and [$Cp^*Ru^{II}\{HB(mt)_3\}$] are designated **1B** and **2B**, respectively). The rate and equilibrium constants associated with the reactions **1A** ⇌ **2A** ⇌ **2B** ⇌ **1B** ⇌ **1A** have been determined by theoretical digital simulation comparisons of experimental ^1H NMR spectroscopic and cyclic voltammetric data over a range of temperatures.

1. Introduction

Conformational changes or ligand substitutions about a metal ion that result in substantial structural changes can occur prior to, during, or after electron-transfer steps.[1,2] If the structural rearrangement occurs simultaneously to the electron transfer, the process is termed a "concerted" single-step (E) reaction, whereas a "consecutive" or "gated" process involves the transformation or chemical step (C) occurring before (CE) or after (EC) the electron transfer.[3,4] Of particular interest among consecutive reactions are those where both the reduced and oxidized species undergo a chemically *reversible* structural change so that a "square scheme" mechanism results (Scheme 1).[1,2,5−14] Often in purely synthetic studies only the final stable product(s) are identified out of solution; consequently, unless the square scheme is specifically looked for, some of the species in Scheme 1

Scheme 1. Electrochemical Consecutive Square Scheme

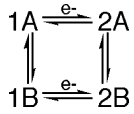

* To whom correspondence should be addressed. E-mail: chmgohly@nus.edu.sg (L.Y.G.); webster@rsc.anu.edu.au (R.D.W.).

(1) Geiger, W. E. *Prog. Inorg. Chem.* **1985**, *33*, 275−352.
(2) Evans, D. H.; O'Connell, K. M. *Electroanal. Chem.* **1986**, *14*, 113−207.
(3) Hoffman, B. M.; Ratner, M. A. *J. Am. Chem. Soc.* **1987**, *109*, 6237−6243.
(4) Brunschwig, B. S.; Sutin, N. *J. Am. Chem. Soc.* **1989**, *111*, 7454−7463.
(5) (a) Bernardo, M. M.; Robandt, P. V.; Schroeder, R. R.; Rorabacher, D. B. *J. Am. Chem. Soc.* **1989**, *111*, 1224−1231. (b) Robandt, P. V.; Schroeder, R. R.; Rorabacher, D. B. *Inorg. Chem.* **1993**, *32*, 3957−3963. (c) Villeneuve, N. M.; Schroeder, R. R.; Ochrymowycv, L. A.; Rorabacher, D. B. *Inorg. Chem.* **1997**, *36*, 4475−4483. (d) Ambundo, E. A.; Ochrymowycv, L. A.; Rorabacher, D. B. *Inorg. Chem.* **2001**, *40*, 5133−5138. (e) Kandegedara, A.; Krylova, K.; Nelson, T. J.; Schroeder, R. R.; Ochrymowycv, L. A.; Rorabacher, D. B. *Dalton Trans.* **2002**, 792−801. (f) Galijasevic, S.; Krylova, K.; Koenigbauer, M. J.; Jaeger, G. S.; Bushendorf, J. D.; Heeg, M. J.; Ochrymowycv, L. A.; Taschner, M. J.; Rorabacher, D. B. *Dalton Trans.* **2003**, 1577−1586.
(6) (a) Evans, D. H. *Chem. Rev.* **1990**, *90*, 739−751. (b) Lerke, S. A.; Evans, D. H.; Feldberg, S. W. *J. Electroanal. Chem.* **1990**, *296*, 299−315. (c) Hong, S. H.; Evans, D. H.; Nelson, S. F.; Ismagilov, R. F. *J. Electroanal. Chem.* **2000**, *486*, 75−84.
(7) (a) Bond, A. M.; Colton, R.; Feldberg, S. W.; Mahon, P. J.; Whyte, T. *Organometallics* **1991**, *10*, 3320−3326. (b) Bond, A. M.; Feldberg, S. W.; Greenhill, H. B.; Mahon, P. J.; Colton, R.; Whyte, T. *Anal. Chem.* **1992**, *64*, 1014−1021.
(8) Araki, K.; Shu, C.-F.; Anson, F. C. *Inorg. Chem.* **1991**, *30*, 3043−3047.
(9) (a) Richards, T. C.; Geiger, W. E. *J. Am. Chem. Soc.* **1994**, *116*, 2028−2033. (b) Wooster, T. T.; Geiger, W. E.; Ernst, R. D. *Organometallics* **1995**, *14*, 3455−3460. (c) Geiger, W. E.; Ohrenberg, N. C.; Yeomans, B.; Connelly, N. G.; Emslie, D. J. H. *J. Am. Chem. Soc.* **2003**, *125*, 8680−8688. (d) Shaw, M. J.; Hyde, J.; White, C.; Geiger, W. E. *Organometallics* **2004**, *23*, 2205−2208.
(10) Hecht, M.; Schultz, F. A.; Speiser, B. *Inorg. Chem.* **1996**, *35*, 5555−5563.
(11) Pierce, D. T.; Hatfield, T. L.; Billo, E. J.; Ping, Y. *Inorg. Chem.* **1997**, *36*, 2959−2955.
(12) Batchelor, R. J.; Einstein, F. W. B.; Gay, I. D.; Gu, J.-H.; Mehta, S.; Pinto, B. M.; Zhou, X.-M. *Inorg. Chem.* **2000**, *39*, 2558−2571.
(13) Fabre, B.; Hapiot, P.; Simonet, J. *J. Phys. Chem. A* **2002**, *106*, 5422−5428.
(14) (a) Svanholm, U.; Bechgaard, K.; Parker, V. D. *J. Am. Chem. Soc.* **1974**, *96*, 2409−2413. (b) Williams, L. L.; Webster, R. D. *J. Am. Chem. Soc.* **2004**, *126*, 12441−12450.

10.1021/om050432o CCC: $30.25
Publication on Web 08/18/2005

may never be detected. In this study a combined synthetic, spectroscopic (NMR), and dynamic electrochemical (cyclic voltammetry) approach is used, enabling characterization of all of the solution-phase species in Scheme 1 and their rates of interconversion.

The homogeneous reactions following electron transfer in Scheme 1 can be first-order conversions such as isomerizations or higher order reactions, such as proton transfers in biological phenolic compounds.[14] There is often difficulty in electrochemically recognizing a square scheme if the chemical steps are relatively fast, and the equilibrium constants favor the primary species produced during electron transfer, so that cyclic voltammograms performed at slow scan rates simply appear the same as that observed for a reversible electron transfer (E step), with no apparent follow-up chemical reactions. Such behavior has been observed for Cu^{II}/Cu^{I}-(L) systems[5] and during the *cis*−*trans* or *fac*−*mer* isomerization of metal carbonyl complexes,[7] where low temperatures and fast voltammetric scan rates (kV s^{-1}) were necessary to detect the species produced by homogeneous reaction. Variations in the electrochemical data with changing concentration are an indication of whether the chemical steps in the square scheme occur through an intermolecular (such as ligand exchange or proton transfer)[8,10,14] or intramolecular process (such as conformational change).[5,6c,7−9,11−13] However, there is also the possibility that concentration dependence can result from a solution electron transfer (SET) mechanism, which can occur through the homogeneous cross-reaction in Scheme 1:[9a]

$$\mathbf{1A} + \mathbf{2B} \rightleftharpoons \mathbf{2A} + \mathbf{1B} \qquad (1)$$

Quantification of the homogeneous and heterogeneous rates of reactions examined by cyclic voltammetry has been made easier over the past decade by the availability of digital simulation software packages such as DigiSim, which enables rapid comparisons of theoretical models with the experimental data.[15] In this study, cyclic voltammetry is used to quantify the rates of isomerization of Ru^{II}/Ru^{III} organometallic compounds containing the hydrotris(methimazolyl)borate ligand, $HB(mt)_3$.

The $HB(mt)_3$ anion (also abbreviated as Tm^R)[16] is an S_3-donor analogue of Trofimenko's versatile N_3-donor poly(pyrazolyl)borates ("scorpionates"), Tp^R [17] (Chart 1). Intense interest has been generated in $HB(mt)_3$ and the allied compound $H_2B(mt)_2$ (also abbreviated as Bm^R)[18] as ligands, and their coordination chemistry has been rapidly developed by the groups of Reglinski, Spicer, Parkin, and others. To date, complexes of the types $M(Tm^R)_2$ and $M(Bm^R)_2$ are known for the first-row transition metals of groups 8−11, the group 12 metals, and the main-group elements Sn, Pb, As, Bi, and Te.[18,19] Also well characterized are compounds of the type $M(Tm^R)$ (M = Ag(I), Tl(I), Pb(II), $Mo(CO)_2(\eta^3$-allyl), $W(CO)_3I$)[20] and of the type $[M(Tm^R)X]$ (X = Cl, Br, I; M = Zn, Cd, Hg,[21] M = Co(II)[19d]). Notably, the successful isolation of the unusual Bi(III) cation $[Bi(Tm^R)_2]^+$ demonstrated that Tm^R is the softest in the series of 6e donor ligands, indicating a softness order of Tm^R > Cp > Tp^R for the face-capping ligands.[18]

Several groups have capitalized on the tripodal "tetrahedral enforcing" nature of these S_3 ligands to generate coordination compounds of group 12 metals suitable for use as biomimetic models of the zinc enzyme liver

Chart 1. Sulfur-Containing Analogues of Trofimenko's Polypyrazolylborate Ligand, $HB(pz)_3$

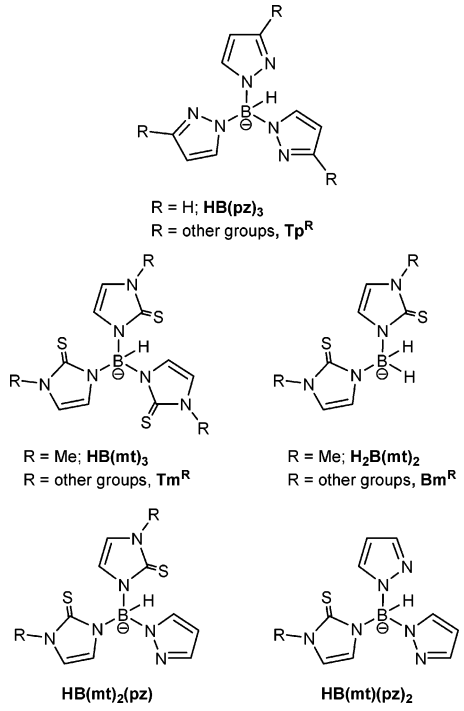

(15) (a) DigiSim; Bioanalytical Systems, Inc. (BAS), 2701 Kent Ave., West Lafayette, IN 47906. (b) Rudolph, M.; Reddy, D. P.; Feldberg, S. W. *Anal. Chem.* **1994**, *66*, 589A−600A.

(16) (a) Garner, M.; Reglinski, J.; Cassidy, I. D.; Spicer, M. D.; Kennedy, A. R. *Chem. Commun.* **1996**, 1975−1976. (b) Reglinski, J.; Garner, M.; Cassidy, I. D.; Slavin, P. A.; Spicer, M. D.; Armstrong, D. R. *J. Chem. Soc., Dalton Trans.* **1999**, 2119−2126.

(17) (a) Trofimenko, S. *J. Am. Chem. Soc.* **1966**, *88*, 1842−1844. (b) Trofimenko, S. *J. Am. Chem. Soc.* **1967**, *89*, 3170−3177. (c) Trofimenko, S. *Chem. Rev.* **1993**, *93*, 943−980. (d) Trofimenko, S. *Scorpionates: The Coordination Chemistry of Polypyrazolylborate Ligands*; Imperial College Press: London, 1999, and references therein. (e) Trofimenko, S. *Polyhedron* **2004**, *23*, 197−203. (f) Pettinari, C.; Santini, C. *Comprehensive Coordination Chemistry II*; Elsevier: Oxford, U.K., 2003, Vol. 1, pp 159−208. (g) Trofimenko, S. *Prog. Inorg. Chem.* **1986**, *34*, 115−210.

(18) Reglinski, J.; Spicer, M. D.; Garner, M.; Kennedy, A. R. *J. Am. Chem. Soc.* **1999**, *121*, 2317−2318.

(19) (a) Garner, M.; Lewinski, K.; Pattek-Janczyk, A.; Reglinski, J.; Sieklucka, B.; Spicer, M. D.; Szaleniec, M. *Dalton Trans.* **2003**, 1181−1185. (b) Mihalcik, D. J.; White, J. L.; Tanski, J. M.; Zakharov, L. N.; Yap, G. P. A.; Incarvito, C. D.; Rheingold, A. L.; Rabinovich, D. *Dalton Trans.* **2004**, 1626−1634. (c) Dodds, C. A.; Lehmann, M.-A.; Ojo, J. F.; Reglinski, J.; Spicer, M. D. *Inorg. Chem.* **2004**, *43*, 4927−4934. (d) Kimblin, C.; Bridgewater, B. M.; Hascall, T.; Parkin, G. *Dalton Trans.* **2000**, 1267−1274. (e) Slavin, P. A.; Reglinski, J.; Spicer, M. D.; Kennedy, A. R. *Dalton Trans.* **2000**, 239−240. (f) Dodds, C. A.; Jagoda, M.; Reglinski, J.; Spicer, M. D. *Polyhedron* **2004**, *23*, 445−450. (g) Bridgewater, B. M.; Parkin, G. *Inorg. Chem. Commun.* **2000**, *3*, 534−536. (h) Dodds, C. A.; Kennedy, A. R.; Reglinski, J.; Spicer, M. D. *Inorg. Chem.* **2004**, *43*, 394−395. (i) Alvarez, H. M.; Tran, T. B.; Richter, M. A.; Alyounes, D. M.; Rabinovich, D.; Tanski, J. M.; Krawiec, M. *Inorg. Chem.* **2003**, *42*, 2149−2156.

(20) (a) Santini, C.; Lobbia, G.; Pettinari, C.; Pellei, M.; Valle, G.; Calogero, S. *Inorg. Chem.* **1998**, *37*, 890−900. (b) Santini, C.; Pettinari, C.; Lobbia, G.; Spagna, R.; Pellei, M.; Vallorani, F. *Inorg. Chim. Acta* **1999**, *285*, 81−88. (c) Ojo, J. F.; Slavin, P. A.; Reglinski, J.; Spicer, M. D.; Garner, M.; Kennedy, A. R.; Teat, S. J. *Inorg. Chim. Acta* **2001**, *313*, 15−20. (d) Bridgewater, B. M.; Parkin, G. *J. Am. Chem. Soc.* **2000**, *122*, 7140−7141. (e) Garner, M.; Lehmann, M.; Reglinski, J.; Spicer, M. D. *Organometallics* **2001**, *20*, 5233−5236.

(21) (a) Cassidy, I.; Garner, M.; Kennedy, A. R.; Potts, G. B. S.; Reglinski, J.; Slavin, P. A.; Spicer, M. D. *Eur. J. Inorg. Chem.* **2002**, 1235−1239. (b) Bakbak, S.; Bhatia, V. K.; Incarvito, C. D.; Rheingold, A. L.; Rabinovich, D. *Polyhedron* **2001**, *20*, 3343−3348. (c) White, J. L.; Tanski, J. M.; Rabinovich, D. *Dalton Trans.* **2002**, 2987−2991.

alcohol dehydrogenase (LADH).[22] In a search for the closest coordination model of Zn in LADH (which involves one histidine and two cysteine residues), Vahrenkamp and Parkin trialed compounds containing a S_2N environment provided by hybrid $mt_2pz-pzBm^R$ hydroborate ligands (see Chart 1)[19d,23] or Bm^R with an N coligand.[24] Re(I) and Tc(I) compounds containing *fac*-$M(CO)_3$ fragments coordinated to Tm^R or Bm^R are of relevance to the development of new radiopharmaceuticals.[25] Other organometallic compounds include $(Tm^R)Mn^I(CO)_3$ and the Ru(II) compounds $[(Tm^R)Ru(p\text{-cymene})]Cl$ and $[(Tm^R)RuCp]$,[26] the tin(IV) complexes $[(Tm^R)R_xSnCl_y]$ ($x = 1-3$; $y = 3 - x$),[27] anionic species $[Mo(CO)_3(Tm^R)]^-$ and $[Mo(CO)_4(Bm^R)]^-$,[28a] and Tm^R alkylidyne complexes of W.[28b] Very recent papers have reported metallaboratranes containing a dative M→B bond for Co,[19b] Ru,[28c,d] Os,[28e] Pt(0) and Pt(II),[28f] and Rh(I).[28g]

Geiger et al. reported the electrochemistry of $[LL'Rh^{I/II}(Tp^{Me2})]$ complexes, where L = CO, PPh_3 and L′ = $P(OPh)_3$, PPh_3, PCy_3.[9c] The Rh(II) compounds were known to favor κ^3 bonding in Tp^{Me2} (through three nitrogen atoms), resulting in five-coordinate complexes, whereas the Rh(I) complexes favored κ^2 bonding in Tp^{Me2} (or an equilibrium between κ^2- and weak κ^3-Tp^{Me2} coordination), producing four-coordinate complexes. The observed cyclic voltammetric responses were interpreted on the basis of the rates of heterogeneous electron transfer. The compounds that displayed slow (irreversible) heterogeneous charge-transfer processes were modeled according to the square scheme in Scheme 1, involving intramolecular associative and dissociative formation/cleavage of the Rh−N bond. Compounds that underwent fast (reversible) heterogeneous electron transfer were consistent with either a concerted (single-step) mechanism or with the chemical steps in Scheme 1 proceeding so quickly that they were indistinguishable from the charge-transfer step.

Scheme 2. κ^3-H,S,S′ Coordination of $[HB(mt)_3]^-$ Anion[28d]

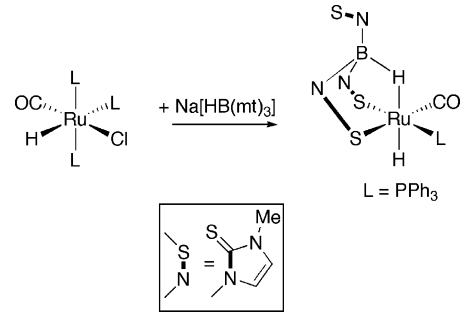

Our interest in the solution-phase chemistry of Tm^R metal complexes arose because of the postulation of bidentate coordination of the ligand via two sulfurs in $[(Tm^R)RuCp]$, on the basis of spectral data[26] and the recent solid-state crystallographic evidence of κ^3-H,S,S′ coordination of Tm in a Ru(II) complex by Hill et al.[28d] (Scheme 2). The predominance of κ^3-H,S,S′ ligation over the normal κ^3-S,S′,S″ coordination mode via all three sulfurs had also been observed for $(Tm^R)Ni^{II}$ complexes.[29] This leads to the possibility of both coordination modes existing in solution and with the equilibrium between the two varying, depending on the oxidation state of the metal. Such processes are ideally studied by dynamic electrochemical techniques that enable cycling between Ru(II) and Ru(III).

2. Experimental Section

2.1. General Procedures. All reactions were carried out using conventional Schlenk techniques under an inert atmosphere of nitrogen or under argon in an M. Braun Labmaster 130 inert gas system. NMR spectra were measured on a Bruker 300 MHz FT NMR spectrometer; ^1H and ^{13}C chemical shifts were referenced to residual C_6H_6 in C_6D_6, CH_2DCN in CD_3CN, or $C_6H_5CD_3$ in d_8-toluene. 2D ^1H NMR spectra (COSY, NOESY, and EXSY) of **2A/2B** were obtained in C_6D_6 on a Bruker DRX 500 MHz FT NMR spectrometer with a triple-resonance cryoprobe head. IR spectra of KBr disks were measured in the range of 4000−600 cm^{-1} by means of a BioRad FTS-165 FTIR instrument. Mass spectra were run on a Finnigan Mat 95XL-T or a Finnigan Mat LCQ spectrometer. Elemental analyses were carried out by the microanalytical laboratory in house. Potassium hydrotris(methimazolyl)borate ($K[HB(mt)_3]$, where $HB(mt)_3 = [(C_4H_5N_2S)_3BH]$), $[Cp^*RuCl_2]_2$, and $[Cp^*RuOMe]_2$ were synthesized as reported in the literature.[30,31]

2-Mercapto-1-methimazolyl was used as purchased from Lancaster Synthesis Ltd., and $RuCl_3{\cdot}3H_2O$ was used as purchased from Pressure Chemical Co. Solvents were dried over sodium benzophenone or calcium hydride and distilled before use. Celite (Fluka AG) and silica gel (Merck Kieselgel 60, 230−400 mesh) were dried at 140 °C overnight before chromatographic use. Conductivity measurements were conducted at 300 K on $(1 \times 10^{-5})-(5 \times 10^{-3})$ M solutions in acetonitrile, using a Kyoto Electronics CM-115 conductivity bridge.

Cyclic voltammetric experiments were conducted with a 1 mm diameter glassy carbon working electrode and a computer controlled Eco Chemie μAutolab III potentiostat. The electrochemical cell was jacketed in a glass sleeve and cooled between

(22) See for instance the following and references therein: (a) Vahrenkamp, H. *Acc. Chem. Res.* **1999**, *32*, 589−596. (b) Tesmer, M.; Shu, M.; Vahrenkamp, H. *Inorg. Chem.* **2001**, *40*, 4022−4029. (c) Parkin, G. *Chem. Commun.* **2000**, 1971−1985. (d) Docrat, A.; Morlok, M. M.; Bridgewater, B. M.; Churchill, D. G.; Parkin, G. *Polyhedron* **2004**, *23*, 481−488.

(23) (a) Seebacher, J.; Shu, M.; Vahrenkamp, H. *Chem. Commun.* **2001**, 1026−1027. (b) Shu, M.; Walz, R.; Wu, B.; Seebacher, J.; Vahrenkamp, H. *Eur. J. Inorg. Chem.* **2003**, 2502−2511. (c) Kimblin, C.; Bridgewater, B. M.; Churchill, D. G.; Hascall, T.; Parkin, G. *Inorg. Chem.* **2000**, *39*, 4240−4243.

(24) (a) Kimblin, C.; Hascall, T.; Parkin, G. *Inorg. Chem.* **1997**, *36*, 5680−5681. (b) Müller, B.; Schneider, A.; Tesmer, M.; Vahrenkamp, H. *Inorg. Chem.* **1964**, *3*, 1900−1907.

(25) (a) Garcia, R.; Paulo, A.; Domingos, A.; Santos, I.; Ortner, K.; Alberto, R. *J. Am. Chem. Soc.* **2000**, *122*, 11240−11241. (b) Garcia, R.; Paulo, A.; Domingos, A.; Santos, I. *J. Organomet. Chem.* **2001**, *632*, 41−48. (c) Garcia, R.; Xing, Y.; Paulo, A.; Domingos, A.; Santos, I. *Dalton Trans*. **2002**, 4236−4241. (d) Garcia, R.; Domingos, A.; Paulo, A.; Santos, I.; Alberto, R. *Inorg. Chem.* **2002**, *41*, 2422−2428. (e) Garcia, R.; Paulo, A.; Domingos, A.; Santos, I. *Dalton Trans.* **2003**, 2757−2759.

(26) Bailey, P. J.; Lorono-Gonzales, D. J.; McCormack, C.; Parsons, S.; Price, M. *Inorg. Chim. Acta* **2003**, *354*, 61−67.

(27) Santini, C.; Pellei, M.; Lobbia, G. G.; Pettinari, C.; Drozdov, A.; Troyanov, S. *Inorg. Chim. Acta* **2001**, *325*, 20−28.

(28) (a) Foreman, M. R. St.-J.; Hill, A. F.; Tshabang, N.; White, A. J. P.; Williams, D. J. *Organometallics* **2003**, *22*, 5593−5596. (b) Foreman, M. R. St.-J.; Hill, A. F.; White, A. J. P.; Williams, D. J. *Organometallics* **2003**, *22*, 3831−3840. (c) Hill, A. F.; Owen, G. R.; White, A. J. P.; Williams, D. J. *Angew. Chem., Int. Ed.* **1999**, *38*, 2759−2761. (d) Foreman, M. R. St.-J.; Hill, A. F.; Owen, G. R.; White, A. J. P.; Williams, D. J. *Organometallics* **2003**, *22*, 4446−4450. (e) Foreman, M. R. St.-J.; Hill, A. F.; White, A. J. P.; Williams, D. J. *Organometallics* **2004**, *23*, 913−916. (f) Crossley, I. R.; Hill, A. F. *Organometallics* **2004**, *23*, 5656−5658. (g) Crossley, I. R.; Foreman, M. R. St.-J.; Hill, A. F.; White, A. J. P.; Williams, D. J. *Chem. Commun.* **2005**, 221−225.

(29) Alvarez, H. M.; Tanski, J. M.; Rabinovich, D. *Polyhedron* **2004**, *23*, 395−403.

(30) Soares, L. F.; Silva, R. M. *Inorg. Synth*. **2002**, *33* 199−202.

(31) Koelle, U.; Kossakowski, J. *Inorg. Synth*. **1992**, *29*, 225−228.

Scheme 3

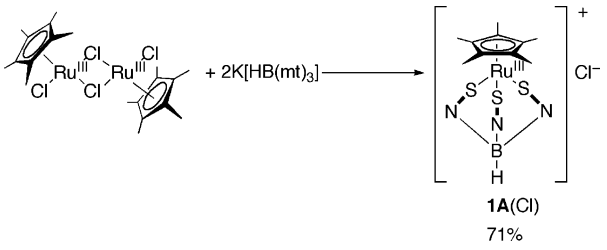

Scheme 4

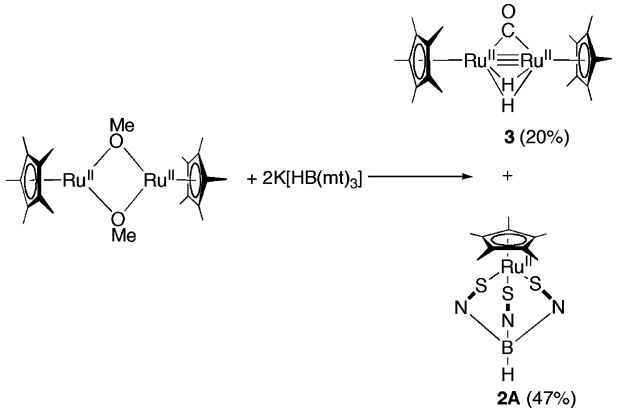

233 and 293 K using a Lauda RL6 variable temperature methanol-circulating bath. Test solutions were thoroughly deoxygenated with argon prior to analysis and a continuous stream of argon was passed over the solution during measurements. The experiments were performed by recording cyclic voltammograms in the presence and absence of substrate. The background-subtracted curves were compared with cyclic voltammetry curves simulated using DigiSim 3.03.[15] Solutions of electrogenerated compounds for the EPR experiments were prepared at 233 K in a two-compartment controlled-potential electrolysis cell separated with a porosity No. 5 (1.0−1.7 μm) sintered-glass frit. The working and auxiliary electrodes were identically sized Pt mesh plates symmetrically arranged with respect to each other with an Ag-wire reference electrode (isolated by a salt bridge) positioned to within 2 mm of the surface of the working electrode. The electrolyzed solutions were transferred under vacuum into cylindrical 3 mm (i.d.) EPR tubes that were immediately frozen in liquid N_2. EPR spectra were recorded on a Bruker ESP 300e spectrometer in a TE_{102} cavity at 10 K using liquid He cooling. EPR simulations were performed using the Bruker computer software WINEPR SimFonia.

2.2. Synthesis. Reaction of [Cp*RuCl]$_2$ with K[HB(mt)$_3$] (Scheme 3). To a brown solution of $[Cp^*RuCl_2]_2$ (31 mg, 0.05 mmol) in THF was added K[HB(mt)$_3$] (39 mg, 0.10 mmol). The suspension was stirred for 18 h. The resultant brown suspension was filtered through a glass sinter to give a dark brown solid product; it was found that some unreacted $[Cp^*RuCl_2]_2$ remained in the mother liquor. The solid was extracted with CH_3CN (4 × 5 mL), leaving behind the KCl byproduct and some residual K[HB(mt)$_3$]. The dark brown extract was concentrated to ca. 3 mL and ether added. After it stood for 2 days at −30 °C, the mixture yielded a dark brown solid of $[Cp^*Ru^{III}\{HB(mt)_3\}]Cl$ (**1A**(Cl); 44 mg, 0.71 mmol, 71% yield). For anion exchange, a solution of **1A**(Cl) (12 mg, 0.02 mmol) in CH_3CN was stirred with excess NH_4PF_6 (7 mg, 0.04 mmol) at room temperature for 3 h. After removal of NH_4Cl by filtration on a glass sinter, the reddish brown filtrate was concentrated to ca. 2 mL and ether added. Dark brown rhombic crystals of **1A**(PF_6) were obtained after 2 days at −30 °C. Anal. Found: C, 41.9; H, 5.0; N, 13.1; S, 15.0. Calcd for $C_{22}H_{31}BClN_6RuS_3$: C, 42.4; H, 5.0; N, 13.5; S, 15.4. ^{1}H NMR: 26.6 (s, br, $\nu^{1/2}$ ca. 90 Hz, ca. 15H, C_5Me_5); 11.2 (s, $\nu^{1/2}$ ca. 5 Hz, ca. 6H, CH, imidazole); 9.8 (s, $\nu^{1/2}$ ca. 6 Hz, ca. 9H, Me, imidazole); B*H* not observed. IR (KBr, cm^{-1}): ν(BH) 2428 w; ν(other bands) 1562 m, 1461 m, 1374 m, 1210 s, 1262 s, 752s. MS FAB$^+$ (*m/z*): 588 [M = $C_5Me_5Ru(C_4H_5N_2S)_3BH]^+$, 474 [M − $C_4H_5N_2S$ − H]$^+$, 350 [M − $(C_4H_5N_2S)_2BH]^+$. MS FAB$^-$ (*m/z*): 351 [M = $(C_4H_5N_2S)_3BH]^-$. HR-MS FAB$^+$ (*m/z*): for [M$^+$] 588.0897 (found), 588.0909 (calcd). The ^{1}H NMR spectrum in CD_3CN shows broad peaks that are in agreement with a paramagnetic d^5 Ru(III) center. The conductivity measurement of **1A**(Cl) in CH_3CN at 300 K gives the molar conductivity Λ_m(1 × 10^{-3} M) = 145.9 Ω^{-1} cm^2 mol^{-1}, which falls in the range (120−160 Ω^{-1} cm^2 mol^{-1}) of a 1:1 electrolyte.[33] The slope of the Onsager plot of $(\Lambda_0 - \Lambda_M)$ vs $c^{1/2}$ = 133.61 × 10^3, where Λ_M and Λ_0 represent molar conductances at concentration *M* and infinite dilution, respectively.

Reaction of [Cp*Ru(OMe)]$_2$ with K[HB(mt)$_3$] (Scheme 4). To a dark pink solution of $[Cp^*Ru(OMe)]_2$ (54 mg, 0.10 mmol) in THF was added K[HB(mt)$_3$] (78 mg, 0.20 mmol). The suspension was refluxed for 6 h, resulting in a brownish red suspension, which was filtered to remove the white KOMe byproduct. The brownish red filtrate was concentrated to ca. 2 mL and chromatographed on a silica gel column packed in hexane (1.5 cm × 8 cm). Elution gave two fractions, leaving behind an immovable brown band on the column. (i) The first fraction was a brownish yellow eluate (2:1 hexane−toluene, 20 mL), which on concentration gave a yellowish brown crystalline solid of $Cp^*Ru(\mu\text{-}H)_2(\mu\text{-}CO)RuCp^*$ (**3**; 10 mg, 0.02 mmol, 20%), identified by a comparison of its ^{1}H NMR spectrum, its CO stretching frequency in the IR spectrum, and the cell parameters of a single crystal with those of an identical compound obtained when $[Cp^*RuOMe]_2$ was heated at temperatures >90 °C in toluene for 4 h.[34a] Data for **3**: space group *Pa*, *a* = 10.027(5) Å, *b* = 8.511 (5) Å, *c* = 12.500 (6) Å, β = 108.64(4)°, *V* = 1010.8 (7) Å^3; ^{1}H NMR (C_6D_6) δ 1.79 (s, 30H), −12.89 (s, 2H); ν (CO, KBr): 1793 cm^{-1}. Lit.[34] data: space group *Pa*, *a* = 12.621(3) Å, *b* = 8.574(2) Å, *c* = 10.089(2) Å, β = 108.56(3)°, *V* = 998.3(3) Å^3; ^{1}H NMR (C_6D_6) δ 1.78 (s, 30H), −12.9 (s, 2H); ν(CO) 1794 cm^{-1}. (ii) The second fraction was a red eluate (1:2 toluene−THF, 50 mL), which upon concentration and addition of hexane gave reddish orange microcrystalline solids, $[Cp^*Ru^{II}\{HB(mt)_3\}]$ (**2A**; 55 mg, 0.09 mmol, 47% yield), after 1 day at −30 °C. Anal. Found: C, 46.2; H, 5.6; N, 13.5; S, 15.5. Calcd for $C_{22}H_{31}BN_6RuS_3\cdot 0.25C_6H_{12}$: C, 46.5; H, 5.5; N, 13.8; S, 15.8. IR (KBr, cm^{-1}): ν(BH) 2407 w; ν(other bands) 1560 m, 1454 m, 1412 m, 1369 s, 1317 m, 1294 m, 1204 s, 730 m, and 720 m. MS FAB$^+$ (*m/z*): 588.1 [M$^+$ = $C_5Me_5Ru(C_4H_5N_2S)_3BH]$, 474 [M − $C_4H_5N_2S$ − H]$^+$, 350 [M − $(C_4H_5N_2S)_2BH]^+$. FAB$^-$ (*m/z*): 351 [M = $(C_4H_5N_2S)_3BH]^-$. ^{1}H NMR (C_6D_6; assignment of peaks was based on data from the 2D ^{1}H NMR COSY and EXSY spectra (see the Supporting Information)): isomer **2A**, δ 6.58 (d, 3 × 2H, ^3J = 2.5 Hz, SCN_2HC=CH), 5.93 (d, 3 × 2H, ^3J = 2.5 Hz, SCN_2HC=C*H*), 3.16 (s, 3 × 3H, N−CH_3), 1.93 (s, CpCH_3); isomer **2B**, δ 6.47 (d, 2 × 2H, ^3J = 1.6 Hz, SCN_2HC=CH), 6.25 (d, 2H, ^3J = 1.6 Hz, SCN_2HC=CH), 6.01 (d, 2H, ^3J = 1.6 Hz, SCN_2HC=C*H*), 5.78 (d, 2 × 2H, ^3J = 1.6 Hz, SCN_2HC=C*H*), 3.29 (s, 3H, NCH_3), 2.83 (s, 2 × 3H, NCH_3), 1.93 (s, $CpCH_3$), −7.67 (q of equal intensity, 1H, *J* = 48 Hz, μ-HB); approximately relative ratio of **2A:2B** = 1:3 from signal integrals. ^{1}H NMR (CD_2Cl_2; indicative of **2B**): 6.70 (d, 1H, ^3J = 2.5 Hz, CH imidazole), 6.67 (d, 2H, ^3J = 2.5 Hz, CH imidazole), 6.58 (d, 2H, ^3J = 1.7 Hz, CH imidazole), 6.38 (d, 1H, ^3J = 1.7 Hz, CH imidazole, 3.53 (s, 6H, NCH_3), 3.50 (s, 3H, NCH_3), 1.63 (s, 15H, $CpCH_3$), −8.16 (q of equal

(32) Koelle, U.; Kossakowski, J. *J. Chem. Soc., Chem. Commun.* **1988**, 549−551.
(33) Geary, W. J. *Coord. Chem. Rev*. **1971**, *7*, 81−122.
(34) (a) Kang, B.-S.; Koelle, U.; Thewait, U. *Organometallics* **1991**, *10*, 2569−2573. (b) Forrow, N. J.; Knox, S. A. R. *Chem. Commun.* **1984**, 679−681.

intensity, 1H, J 81 Hz, μ-HB). ^{1}H NMR (CD_3CN; indicative of **2B**): 6.84 (d, 1H, ^3J = 1.7 Hz, CH imidazole), 6.82 (d, 2H, ^3J = 1.7 Hz, CH imidazole), 6.69 (d, 2H, ^3J = 1.7 Hz, CH imidazole), 6.36 (d, 1H, ^3J = 1.7 Hz, CH imidazole), 3.49 (s, 6H, NCH_3), 3.46 (s, 3H, NCH_3), 1.92 (s, 15H, $CpCH_3$), −8.27 (q of equal intensity, 1H, J = 81 Hz, μ-HB). ^{13}C NMR (C_6D_6): isomer **2A**, δ 169.4 (s, $SCN_2HC{=}CH$), 120.6 (s, C imidazole), 120.4 (s, C imidazole), 76.1 (s, $C_5(CH_3)_5$), 34.9 (s, NCH_3) 11.5 (s, $C_5(CH_3)_5$); isomer **2B**, δ 169.4 (s, $SCN_2HC{=}CH$), 120.6 (s, C imidazole), 120.4 (s, C imidazole), 79.8 (s, $C_5(CH_3)_5$), 35.0 (s, 2 × NCH_3), 34.4 (s, NCH_3), 11.7 (s, $C_5(CH_3)_5$).

2.3. X-ray Structure Determinations. Diffraction-quality single crystals were obtained at −30 °C as follows: **1A**(PF_6) as dark brown rhombic crystals by slow diffusion of ether in an acetonitrile solution after 5 days; **2A** as pink hexagons from a solution in THF−ether, and **3** as purplish brown rhombic crystals from a THF−hexane solution, after 3 days.

The crystals were mounted on glass fibers. X-ray data were collected on a Bruker APEX AXS diffractometer, equipped with a CCD detector, using Mo Kα radiation (λ = 0.710 73 Å). The program SMART[36] was used for collecting frames of data, indexing reflections, and determination of lattice parameters, SAINT[36] for integration of the intensity of reflections, scaling, and correction of Lorentz and polarization effects, SADABS[37]for absorption correction, and SHELXTL[38] for space group and structure determination and least-squares refinements on F^2. The structures of **1A**(PF_6) and **2A** were solved by direct methods to locate the heavy atoms, followed by difference maps for the light non-hydrogen atoms. Compound **1A**(PF_6) exhibited disorder of the $[PF_6]^-$ anion. This was modeled as a disorder involving four of the F atoms lying in a square plane. These four F atoms were modeled as comprising two sets, with occupancies of the two sets summed to unity. The F atoms in each set were restrained to be in a plane, and all nearest-neighbor F···F distances were restrained to be the same. Diagonally opposing F atoms were given equivalent anisotropic thermal parameters. There was disorder of the Cp* ligand in **2A**. This was modeled with a complete Cp* with one-third occupancy. Since the molecule sits on a 3-fold axis, this automatically generated three alternative sites which are symmetry related, for the entire ligand. The $C_{ring}-C_{methyl}$ bond lengths were all restrained to be the same. All the ring carbon atoms were given a common isotropic thermal parameter, as were all the methyl carbon atoms. The hydrogen atoms were placed and refined in a riding model. There was also half a water solvent molecule found; the hydrogen atoms for this were modeled as disordered over two alternative sites of equal occupancies.

The crystal data collection and processing parameters are given in Table S1 (Supporting Information), and selected bond parameters are given in Table 1.

3. Results and Discussion

3.1. X-ray Structures. The molecular structures of the monocationic Ru(III) complex **1A** and the neutral Ru(II) complex **2A** are markedly similar, each containing a ruthenium center sandwiched between a Cp* ring and a tripodal trisulfur-bonding [HB(mt)$_3$] ligand. They crystallize in monoclinic triclinic $P\bar{1}$ and trigonal $P\bar{3}$ space groups, respectively.

The molecular structures are depicted in parts a and b of Figure 1. **1A** is the first example of a Ru^{III}[HB(mt)$_3$] species reported to date. Bailey and co-workers had prepared an arene Ru(II) analogue of **1A**, [(*p*-cymene)-Ru^{II}{HB(mt)$_3$}]Cl, and the Cp analogue of **2A** from the reaction of Na[HB(mt)$_3$] with [(*p*-cymene)$RuCl_2]_2$ and [$CpRu(MeCN)_3$]PF_6, respectively.[26]

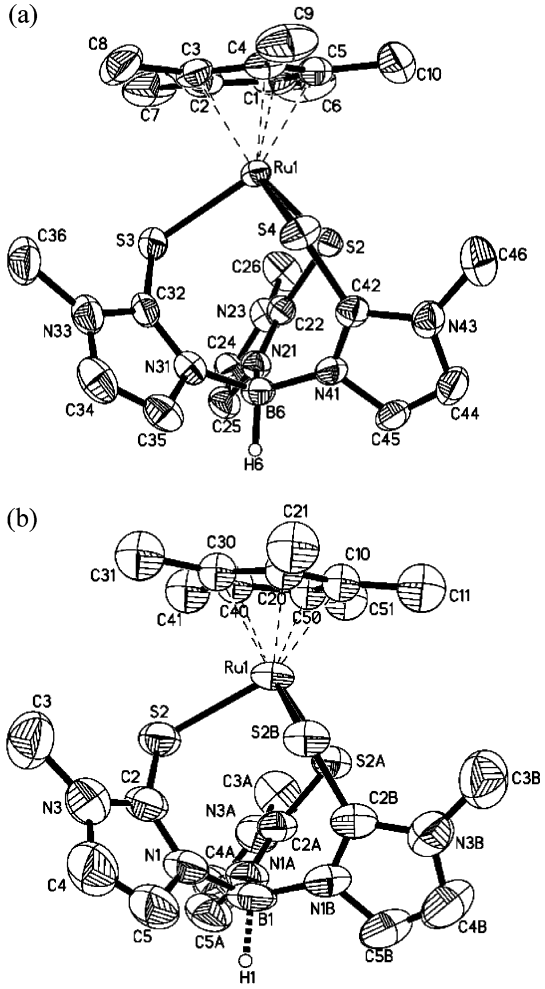

Figure 1. ORTEP plots for the molecular structures of (a) the **1A** monocation and (b) **2A** (a selected view which omits the disorder in Cp*). Thermal ellipsoids are drawn at the 50% probability level for **1A** and the 30% probability level for **2A**. Hydrogen atoms on the Cp*, methimazole, and NMe groups are omitted for clarity.

Table 1. Selected Bond Lengths (Å) and Bond Angles (deg)

Compound **1A**			
Bond Distances			
Ru(1)−S(2)	2.3956(8)	C(22)−S(2)	1.724(3)
Ru(1)−S(3)	2.4100(8)	C(32)−S(3)	1.722(3)
Ru(1)−S(4)	2.3213(8)	C(42)−S(4)	1.724(3)
Ru(1)−Cp* centroid	1.848(1)		
Bond Angles			
S(1)−Ru(1)−(S2)	92.98(3)	Ru(1)−S(2)−C(22)	109.14(10)
S(2)−Ru(1)−S(4)	92.58(3)	Ru(1)−S(3)−C(32)	104.55(11)
S(3)−Ru(1)−S(4)	100.62(3)	Ru(1)−S(4)−C(42)	111.76(10)
Compound **2A**			
Bond Distances			
Ru(1)−S(2)	2.440(2)	C(11)−S(2)	1.72(1)
Ru(1)−Cp* centroid	1.78(1)		
Bond Angles			
S(2)−Ru(1)−S(2A)	92.6(1)	Ru(1)−S(2)−C(2)	110.3(3)

(35) Budzelaar, P. H. M. *g*NMR, version 4.1; Adept Scientific plc.: Amor Way, Letchworth, Herts SG6 1ZA, U.K., 1995−1999.

(36) *SMART & SAINT Software Reference Manuals*, *Version 6.22*; Bruker AXS Inc.: Madison, WI, 2000.

(37) Sheldrick, G. M. SADABS Software for Empirical Absorption Correction; University of Göttingen, Göttingen, Germany, 2000.

(38) *SHELXTL Reference Manual, version 5.1*; Bruker AXS Inc.: Madison, WI, 1997.

Table 2. Variation of 2A:2B[a] with Solvent Composition

C_6D_6:CD_2Cl_2	1:0	0.8:0.2	0.4:0.15	0:1
2A:**2B**	1:3	1:5	1:19	0:1

[a] Obtained from integral ratios of ^{1}H NMR spectra.

Scheme 5. Equilibrium I

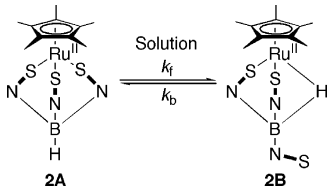

The unit cells of both **1A** and **2A** contain two molecules; that of the latter also contains 0.5 H_2O solvent molecules. There is no plane of symmetry within the structure of **1A**, but **2A** possesses a 3-fold axis brought about by a disorder in the Cp* ligand. The 3-fold axis passes through the center of the Cp* ring and cuts through Ru(1) and B(1).

The bond parameters of **1A** and **2A** are given in Table 1. The Ru−S distances in **1A** are comparable to those in Bailey's [(*p*-cymene)Ru{HB(mt)$_3$}]Cl (range 2.3931(7)−2.4222(7) Å),[26] while those in **2A** are closer to those reported by Hill and co-workers in [RuH(CO)(PPh$_3$){κ^3-*H*,*S*,*S*′-HB(mt)$_3$}] and the ruthenaboratrane complex (ranges 2.4448(11)−2.470(2) and 2.4066(14)−2.4857(14) Å, respectively).[28c] The Ru−S distances in **1A** also closely resemble those (range 2.3396(10)−2.3851(10) Å) found in [(η^6-C_6Me_6)Ru^{II}(9S3)][39a] and [(η^5-C_5Me_5)Ru^{III}(9S3)]PF_6[39b] (9S3 = trithiacyclononane), in which 9S3 is a tripodal S_3 ligand, not unlike [HB(mt)$_3$]. The Ru−Cp*(centroid) distances in **1A** and **2A** are 1.848(1) and 1.78(1) Å, respectively. The C−S bonds of both molecules fall in the range 1.722(3)−1.724(3) Å, intermediate between values of a single bond (ca. 1.81 Å) and a double bond (ca. 1.56 Å),[40]as commonly found in metal complexes of Tm^R.[16,19]

3.2. NMR Studies. The ^{1}H NMR spectrum of a solid sample of **2A** dissolved in C_6D_6 at 293 K shows six doublets for imidazole ring protons and three singlets for the NMe protons, which is more complex than that expected for a κ^3-S,S′S″ coordination mode of the [HB(mt)$_3$] ligand, as determined by X-ray crystallography (Figure 1b). A spectrum in CD_2Cl_2 or CD_3CN shows cleanly the presence of only one species containing two types of "mt" moieties in the relative proportion 2:1, indicative of bidentate coordination of the sulfurs, i.e., κ^3-H,S,S′ coordination of the ligand, as in species **2B**. ^{1}H NMR spectra in different C_6D_6/CD_2Cl_2 compositions showed that the **2A:2B** ratio varied from 1:3 in pure d_6-benzene to 0:1 in pure CD_2Cl_2 (Table 2), indicative of an equilibrium (Scheme 5) between **2A** and **2B**, with relative amounts of **2A** versus **2B** higher in nonpolar solvents such as C_6D_6 and d_8-toluene than in polar solvents such as CD_2Cl_2 and CD_3CN. However, only the form **2A** was obtained in the crystalline state, even when crystallized from acetonitrile/ether. Bailey et al. had postulated a bidentate coordination of the ligand in the Cp analogue of **2A**, on the basis of its ^{1}H NMR spectrum in DMSO.[26]

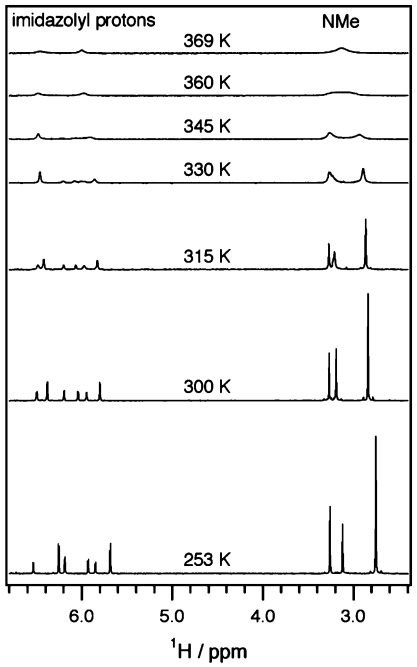

Figure 2. Variable-temperature 300 MHz ^{1}H NMR spectra of **2A/2B** in d_8-toluene.

A VT NMR spectral study of **2A/2B** was conducted on a 0.0170 M solution in d_8-toluene in the temperature range 253−369 K (Figure 2). At 253 K, there were six sets of doublets and three sets of singlets observed for the imidazole ring protons and the NMe protons, respectively. These were assigned to either **2A** or **2B** from 2D ^{1}H COSY and NOESY NMR spectra (see Figures S1 and S2 in the Supporting Information). As the temperature was raised, the NMe signals converged and, at 330 K, the NMe signal belonging to **2A** had coalesced with that of the nonbonded methimazolyl ring, resulting in only two broad signals for both **2A** and **2B**. Finally, at 360 K, these broad singlets collapsed into a single broad "band" ($\nu_{1/2}$ = ca. 92 Hz). Simultaneously, there also occurred the merging of resonances of the imidazole ring protons below 300 K, and at 360 K only two broad peaks ($\nu_{1/2}$ = ca. 29 Hz each) remained. Integrals of the NMe peaks of **2A** and **2B** gave relative concentrations of each species in solution at each temperature, except at 360 and 369 K, when the peaks merged. Hence, the relative concentrations of species at these temperatures were obtained by extrapolation of the linear (R_2 = ca. 1) concentration vs temperature plot in the range 253−345 K. K_{eq} values listed in Table 3 were calculated directly from the [**2B**]/[**2A**] integral ratios. The thermodynamic parameters $\Delta H°$ (−6.38(14) kJ mol^{-1}) and $\Delta S°$ (−13.4(5) J mol^{-1} K^{-1}) were obtained from a plot of ln K_{eq} vs (1/T) (ln K_{eq} = $-(\Delta H°/RT)$ + $(\Delta S°/R)$), and the $\Delta G°$ value (−2.37(14) kJ mol^{-1} for 300 K) was calculated from the equation $\Delta G° = \Delta H° - T\Delta S°$. The negative $\Delta G°$ value is in agreement with the observed facile forward reaction, leading to a high proportion of **2B** in solution. Thermochemical data for organometallic compounds are sparse, but comparison

(39) (a) Shin, R. Y. C.; Bennett, M. A.; Goh, L. Y.; Chen, W.; Hockless, D. C. R.; Leong, W. K.; Mashima, K.; Willis, A. C. *Inorg. Chem.* **2003**, *42*, 96−106. (b) Goh, L. Y.; Teo, M. E.; Khoo, S. B.; Leong, W. K.; Vittal, J. J. *J. Organomet. Chem.* **2002**, *664*, 161−169.

(40) Pauling, L. *The Nature Of The Chemical Bond*, 3rd ed.; Cornell University Press: Ithaca, NY, 1960; Chapter 8, pp 268, 274.

Table 3. Kinetic Data and Equilibrium Constants in d_8-Toluene for Equilibrium I (Scheme 5)

	2A ⇌ 2B				
T/K	rate[a] (**2A** → **2B**)/ mol L^{-1} s^{-1}	k_f[a]/s^{-1}	k_b[a]/s^{-1}	K_{eq}[a]	K_{eq}[b]
369	63	1.0×10^4	5.8×10^3	1.7	1.6
360	38	6.6×10^3	3.3×10^3	2.0	1.7
345	12	2.1×10^3	1.0×10^3	2.1	1.9
330	3.0	5.6×10^2	2.6×10^2	2.2	2.0
315	5.8×10^{-1}	1.2×10^2	48	2.5	2.2
300	7.5×10^{-3}	1.7	6.0×10^{-1}	2.8	2.6
273	1.0×10^{-4}	2.3×10^{-2}	8.0×10^{-3}	2.9	3.3
263					3.7
253					4.2

[a] Obtained by simulation of ^{1}H NMR data using *g*NMR (version 4.1). [b] Obtained from integration ratios of ^{1}H NMR data.

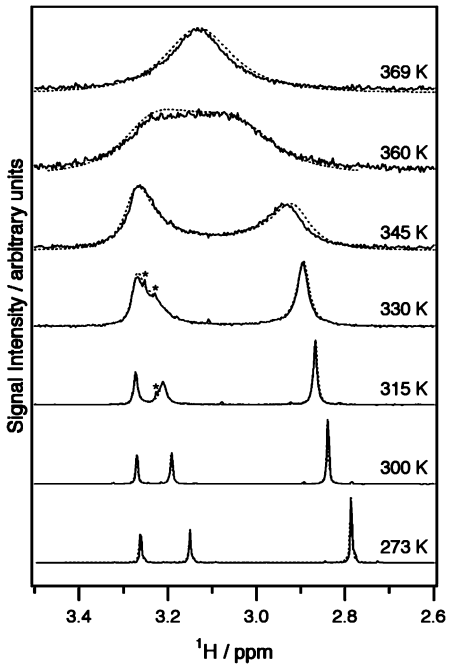

Figure 3. Experimental (solid line) and simulated (dashed line) variable-temperature 300 MHz ^{1}H NMR spectra of **2A/2B** in d_8-toluene. The peaks denoted by asterisks are due to traces of impurities.

of metal−hydride[41] with metal−sulfur[42] bond enthalpies for Cp_2WX (where X = H, S) suggests that the latter are weaker.

The VT ^{1}H NMR spectra in d_8-toluene of the NMe groups were compared with simulations performed using the *g*NMR software[35] in order to obtain additional kinetic and thermodynamic parameters for the intramolecular exchange process (Scheme 5). The natural line widths used were obtained from the spectrum at 253 K, and there was essentially no exchange from temperatures below 273 K. The exchange rates were set and adjusted such that a reasonable fit was obtained between the calculated and experimental spectra (Figure 3). The rate constants, k_f and k_b, were then obtained from the equations rate = k_f[**2A**] and rate = k_b[**2B**], respectively (Table 3). A linear fit using the least-squares method with variance r^2 was obtained from an

Table 4. Thermodynamic Parameters Obtained from Eyring Plots for Equilibrium I (Scheme 5)

	$\Delta H_f^{\ddagger}$/ kJ mol^{-1}	$\Delta S_f^{\ddagger}$/ J mol^{-1} K^{-1}	$\Delta G_f^{\ddagger}$/ kJ mol^{-1}	$\Delta H_b^{\ddagger}$/ kJ mol^{-1}	$\Delta S_b^{\ddagger}$/ J mol^{-1} K^{-1}	$\Delta G^{\ddagger}$/ kJ mol^{-1}	$\Delta G°$/ kJ mol^{-1}
d_8-toluene[a]	114(9)	147(27)	70(9)	119(9)	154(27)	73(9)	−2(9)
CH_2Cl_2[b]	67(4)	0(13)	67(4)	78(3)	11(12)	74(3)	−7(5)

[a] Obtained by simulation of ^{1}H NMR data using *g*NMR (version 4.1). [b] Obtained by simulation of CV data using DigiSim (version 3.03).

Scheme 6. Suggested Mechanism for the 2A/2B Exchange Involving a Solvent-Coordinated Intermediate

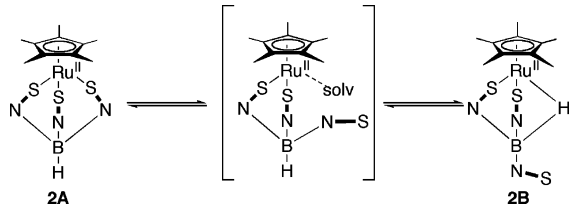

Eyring plot, to afford the thermodynamic parameters (Table 4). A similar Eyring plot was also applied to the CV data (see below). That these values are reasonable has been checked by comparing the derived $\Delta H°$ and $\Delta S°$ values with those obtained from a van't Hoff plot discussed above.

The thermodynamic values given in Table 4 are in agreement with the strong solvent dependence of the **2A/2B** equilibrium (Table 2). The activation enthalpies in Table 4 are also revealing, since they are positive in both solvents but very much more so in d_8-toluene. The implication is that an intermediate species exists between **2A** and **2B** that is more disordered than either **2A** or **2B**. Furthermore, the much smaller $\Delta S^{\ddagger}$ value in CH_2Cl_2 as compared to that in d_8-toluene suggests that there is a significant solvation effect in the intermediate, which is consistent with an exchange mechanism depicted in Scheme 6. It may be expected that the more polar solvent (CH_2Cl_2) would interact more strongly with the Ru center in the intermediate, while toluene (or benzene) does not favor such coordination. Examples of CH_2Cl_2 acting as a ligand are known,[43] and such a picture of the intermediate is also consistent with the larger activation enthalpy in toluene compared to that in CH_2Cl_2, as solvation in the latter would compensate for the cleavage of the Ru−S bond in the intermediate.

3.3. Cyclic Voltammetry. In addition to the equilibrium between **2A** and **2B** that was identified by NMR spectroscopy, CV experiments enabled kinetic quantification of the complete thermodynamic square scheme involving ligand rearrangement about the central Ru atom, following reduction of **1A** and oxidation of **2B** (Scheme 7). The electrochemical experiments were performed in CH_2Cl_2 rather than CH_3CN in order to avoid complications to the square scheme mechanism that could arise through CH_3CN irreversibly coordinating to the ruthenium. Cyclic voltammograms of **1A** at a scan rate of 0.1 V s^{-1} between 233 and 293 K are given in Figure 4a. At 233 K, the CV shows a chemically

(41) Martinho Simões, J. A.; Beauchamp, J. L. *Chem. Rev.* **1990**, *90*, 629−688.
(42) Calhorda, M. J.; de C. T. Carrondo, M. A. A. F.; Dias, A. R.; Domingos, A. M. T. S.; Martinho Simões, J. A.; Teixeira, C. *Organometallics* **1986**, *5*, 660−667.
(43) (a) Tellers, D. M.; Yung, C. M.; Arndtsen, B. A.; Adamson, D. R.; Bergman, R. G. *J. Am. Chem. Soc.* **2002**, *124*, 1400−1410. (b) Huhmann-Vincent, J.; Scott, B. L.; Kubas, G. J. *Inorg. Chem.* **1999**, *38*, 115−124.

Scheme 7. Voltammetric Square Scheme[a]

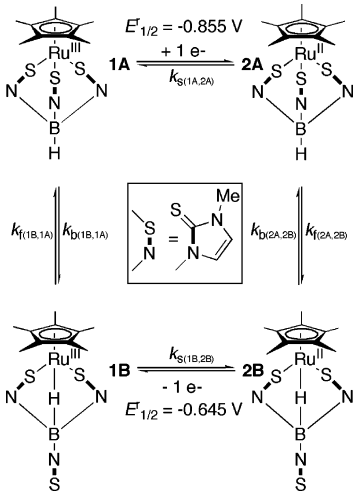

[a] Listed potentials (vs Fc/Fc^+) were obtained by voltammetry. Equilibrium and rate constants are given in Table 5.

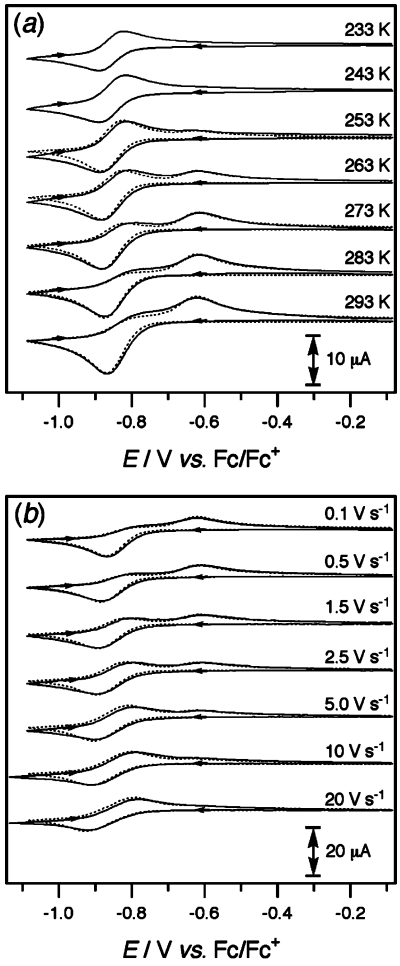

Figure 4. Cyclic voltammograms of 2.36 mM **1A** in CH_2Cl_2 with 0.5 M n-Bu_4NPF_6: (a) scan rate (v) = 0.1 V s^{-1}; (b) T = 293 K. Current data were scaled by multiplying by $v^{-0.5}$. The solid lines denote experimental data, and the dotted lines denote voltammograms simulated using DigiSim.

reversible one-electron reduction process at −0.855 V vs Fc/Fc^+ involving Ru(III) converting to Ru(II) (Scheme 7, **1A** → **2A**). As the temperature was raised, the anodic peak current (i_p^{ox}) associated with the reverse oxidation process (Scheme 7, **2A** → **1A**) diminished in size and an additional oxidation process became evident at a less negative potential (−0.645 V vs Fc/Fc^+). The new oxidation process at −0.645 V vs Fc/Fc^+ was assigned to the oxidation of **2B** that forms via an intramolecular ligand exchange (Scheme 7, **2A** → **2B**). Therefore, the CV's in Figure 4 represent the series of reactions

$$\mathbf{1A} \underset{-e}{\overset{+e}{\rightleftharpoons}} \mathbf{2A} \underset{k_b(\mathbf{2A},\mathbf{2B})}{\overset{k_f(\mathbf{2A},\mathbf{2B})}{\rightleftharpoons}} \mathbf{2B} \underset{+e}{\overset{-e}{\rightleftharpoons}} \mathbf{1B} \qquad (2)$$

By varying the scan rate, the rate constants for the forward and reverse chemical steps in reaction 2 were determined by digital simulation of the CV data over a range of temperatures. Representative data and simulations obtained at 293 K are given in Figure 4b, and the equilibrium and rate constants are listed in Table 5.

Because **2A** is the one-electron-reduced form of **1A**, it could be expected that solutions of **2A** would yield voltammetric processes at a potential identical with that of **1A**, albeit with the current traces offset, because **1A** can be electrochemically reduced while **2A** can be electrochemically oxidized. However, it was observed that solutions prepared from solid samples of crystallographically pure **2A** in CH_2Cl_2 (with 0.5 M Bu_4NPF_6) displayed a major oxidation process ($E^r_{1/2}$) at a potential ∼0.2 V more positive than that of **1A** (Figure 5). Therefore, it was concluded that the main voltammetric process at −0.645 V (vs Fc/Fc^+) was associated with oxidation of **2B** that predominantly forms in solution through the dissolution of **2A** (in agreement with the NMR data above). The CV's obtained for solutions of **2B** were analyzed in a manner similar to that for **1A**. At 233 K, solutions containing **2B** underwent a chemical reversible one-electron-oxidation process involving the transformation of Ru(II) to Ru(III) (Scheme 7, **2B** → **1B**). The CV data at low temperatures (Figure 5a, 233 K) illustrates the stability of the κ^3-H,S,S′ form of [Cp*Ru^{III}-HB(mt)$_3$] (**1B**), since the i_p^{ox}/i_p^{red} value is close to unity. As the temperature was raised, the reverse reduction peak (i_p^{red}) diminished in size and a new process associated with reduction of **1A** become evident at −0.855 V vs Fc/Fc^+ (Figure 5a). Thus, the voltammograms of solutions of **2B** involve the mechanism

$$\mathbf{2B} \underset{+e}{\overset{-e}{\rightleftharpoons}} \mathbf{1B} \underset{k_b(\mathbf{1B},\mathbf{1A})}{\overset{k_f(\mathbf{1B},\mathbf{1A})}{\rightleftharpoons}} \mathbf{1A} \underset{-e}{\overset{+e}{\rightleftharpoons}} \mathbf{2A} \qquad (3)$$

which was modeled over a range of voltammetric scan rates and temperatures analogously to the case for **1A** (Figure 5 and Table 5).

Digital simulations modeled on the CV data obtained during the reduction of solutions of **1A** and oxidation of solutions of **2A/2B** were performed using all four rate

Table 5. Equilibrium, Rate Constants,[a] and Electrochemical Parameters Obtained in CH_2Cl_2 (with 0.5 M Bu_4NPF_6) for the Reaction Given in Scheme 7

			2A ⇌ 2B			**1B ⇌ 1A**		
T/K	$10^{-6}D$/ cm^2 s^{-1}	R/Ω	K_{eq}	k_f/s^{-1}	k_b/s^{-1}	K_{eq}	k_f/s^{-1}	k_b/s^{-1}
293	3.25	800	20	6.00	0.30	205	0.25	1.2×10^{-3}
283	2.5	1000	25	3.25	0.13	220	0.10	4.6×10^{-3}
273	1.95	1200	30	1.00	3.3×10^{-2}	250	0.050	2.0×10^{-4}
263	1.65	1600	35	0.25	7.1×10^{-3}	300	0.025	8.3×10^{-5}
253	1.3	2000	40	0.080	2.0×10^{-3}	380	0.015	3.9×10^{-5}

[a] Obtained by digital simulation of cyclic voltammetry data.

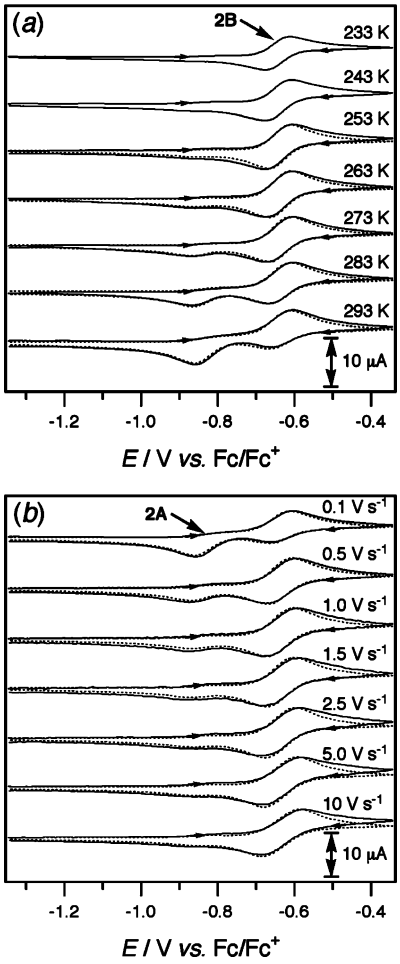

Figure 5. Cyclic voltammograms of 2.61 mM **2A/2B** in CH_2Cl_2 with 0.5 M n-Bu_4NPF_6: (a) scan rate (v) 0.1 V s^{-1}; (b) $T = 293$ K. Current data were scaled by multiplying by $v^{-0.5}$. The solid lines denote experimental data, and the dotted lines denote voltammograms simulated using DigiSim.

constants associated with the two homogeneous chemical reactions given in Scheme 7. Therefore, at any given temperature, the rate and equilibrium constants obtained by simulation were identical regardless of whether the CV's were conducted with solutions of **1A** or **2A/2B**. This self-consistency was necessary in order to confirm the correctness of the square-scheme mechanism. In actuality, digital simulations of the CV's obtained during the reduction of **1A** largely allowed the rate/equilibrium constants associated with the interconversion of species **2A** and **2B**, while simulations modeled on the oxidation of **2B** allowed the rate/equilibrium constants for the interconversion of **1B** and **1A**. One factor that helped to establish the equilibrium constant of the **1B** to **1A** conversion was the presence of a small amount of **2A** (that is, oxidized at −0.855 V vs Fc/Fc^+) together in solution with **2B** at higher temperatures (see Figure 5a, 293 K), which allowed a direct estimation of the K_{eq}(**2A**,**2B**) values (Table 5). (The thermodynamic nature of the square scheme means that if one equilibrium constant (i.e. K_{eq}(**2A**,**2B**)) and both reversible half-wave potentials ($E^r_{1/2}$) (which approximate the formal potential (E^0)) are known, then the second equilibrium constant (i.e. K_{eq}(**1B**,**1A**)) can be automatically calculated.[6c,15])

The increasing anodic (E_p^{ox}) to cathodic (E_p^{red}) peak-to-peak separations (ΔE_{pp}) observed as the scan rate increased (especially at low temperatures) (Figures 4b and 5b) could be adequately accounted for in the simulations by high levels of uncompensated solution resistance in the low conductivity CH_2Cl_2/Bu_4NPF_6 medium. Cyclic voltammograms of solutions of ferrocene that were recorded under identical conditions displayed ΔE_{pp} values that were at least as large as those observed for solutions of **1A** and **2A/2B** (see Figure S6 in the Supporting Information). The voltammetric data did not appear to be affected by slow rates of heterogeneous electron transfer over the scan rates used (that would also increase the ΔE_{pp} values and make extraction of the k_f and k_b values more difficult); thus, the k_s(**1A**,**2A**) and k_s(**1B**,**2B**) values were set at their default values of 10^4 cm s^{-1}. In actuality, with the moderate scan rates used in this study, digital simulations indicate that the k_s values could be as low as approximately 0.05 cm s^{-1}, before the effects of slow heterogeneous electron transfer have a dominating effect on ΔE_{pp} values above the effects of solution resistance. The ΔE_{pp} values increased with increasing concentration (particularly noticeable at higher scan rates and lower temperatures), which supports the conclusion that the relatively high ΔE_{pp} values observed under some conditions were due to uncompensated solution resistance. The diffusion coefficients of **1A** and **1B** were set equal, and the diffusion coefficients of **2A** and **2B** were also set equal and decreased as the temperature was lowered (Table 5). The charge-transfer coefficients (α) were left at their default values of 0.5 eV. The rates of the back homogeneous reactions in Table 5 were often too low to be estimated directly from the variable scan rate data and instead came from knowledge of the k_f and K_{eq} values derived from the simulations.

Varying the concentration between 0.5 and 5 mM led to no observable change in the kinetic values derived from the voltammetric data at a fixed temperature and scan rate, supporting the concept that the ligand exchange occurs via an intramolecular rather than intermolecular mechanism. Below 253 K, the voltammetric peaks associated with the species formed by homogeneous reaction were too small to enable accurate simulations. The variation in the K_{eq} values with changing temperature enabled the reaction enthalpies to be determined from van't Hoff plots, which, for both homogeneous reactions (K_{eq}(**2A**,**2B**) and K_{eq}(**1B**,**1A**)) were calculated to be ∼−10 kJ mol^{-1}. CV experiments performed in mixed CH_2Cl_2/toluene (1:1) indicated a higher **2A/2B** ratio compared to that observed in pure CH_2Cl_2, in agreement with NMR data discussed above (and Table 2), which had indicated that equilibrium I (Scheme 5) favors **2A** in low dielectric media.

3.4. EPR Spectroscopy. Complex **1A** containing a d^5 Ru(III) ion is paramagnetic, and an EPR spectrum was obtained at low temperatures (Figure 6a (solid line)). The EPR signal was very broad and was not detectable above liquid nitrogen temperature, indicating that the unpaired electron was metal rather than ligand centered. The spectrum showed features similar to those expected for species with axial symmetry, albeit with a degree of distortion that was difficult to accurately simulate (see simulation in Figure 6a). It is possible that

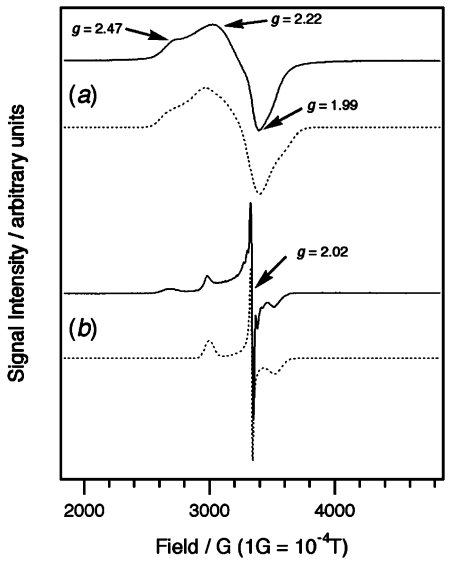

Figure 6. Continuous-wave X-band EPR spectra recorded with microwave frequency 9.44 GHz, microwave power 0.2 mW, modulation amplitude 0.5 mT, time constant 164 ms, sweep width 0.3 T, sweep time 164 s, and $T = 10$ K: (a) (—) **1A** and (- - -) simulated spectrum with 100% Lorentzian line shape and $g_x = 2.37$, $g_y = 2.01$, $g_z = 2.01$, $(\Delta H_{pp})_x = 12$ mT, $(\Delta H_{pp})_y = 13$ mT, $(\Delta H_{pp})_z = 13$ mT, and $a_{Ru} = 4.0$ mT; (b) (—) **1B** and (- - -) simulated spectrum with 100% Lorentzian line shape and $g_x = 2.25$, $g_y = 2.02$, $g_z = 1.91$, $(\Delta H_{pp})_x = 7$ mT, $(\Delta H_{pp})_y = 1$ mT, and $(\Delta H_{pp})_z = 10$ mT.

the experimental spectrum represents several species with slightly differing geometries (due to twisting of the $HB(mt)_3$ ligand), which could also account for the surprisingly large line width that is not typical in Ru(III) compounds. Similar $S = {}^1/_2$ anisotropic spectra have been observed in complexes containing the dithiocarbamate ligand and for octahedral complexes containing bidentate sulfur ligands that have a high degree of covalency and a distorted structure.[44]

Cyclic voltammetry experiments performed at low temperatures indicated that **2A/2B** existed in CH_2Cl_2 in the form of **2B** (Figure 5a). The one-electron oxidation of **2B** produced **1B**, which at 233 K appeared stable on the CV time scale ($v = 100$ mV s^{-1}), since the i_p^{ox}/i_p^{red} ratio was equal to unity. Furthermore, the k_f values given in Table 5 for the **1B** to **1A** isomerization indicate that the reaction occurs slowly at low temperatures; thus, it was thought probable that exhaustive electrolysis of **2B** at 233 K would produce solutions containing mainly **1B**. The solid line in Figure 6b is the EPR spectrum obtained of a frozen solution that was prepared by exhaustive controlled-potential (−0.5 V vs Fc/Fc^+) oxidation of **2B** at 233 K in CH_2Cl_2/0.5 M Bu_4NPF_6 with the transfer of one electron per molecule (measured by coulometry). The spectrum is substantially different from that of **1A** and is dominated by a relatively narrow line width signal centered at $g = 2.02$, which can be explained by the presence of **1B**. Nevertheless, the spectrum is more complicated than would be expected for a single species (see the simulation in Figure 6b) and could contain contamination from a smaller amount of another paramagnetic species. It is possible that **1B** is not indefinitely stable and decomposes or reacts to form an additional paramagnetic Ru^{III} compound on the longer electrolysis time scale. However, any slow decomposition/reaction of **1B** (to a species other than **1A**) is unlikely to have affected the Digisim modeling of the CV data, since the CV experiments were performed over a much shorter time period.

(44) (a) Hall, G. R.; Hendrickson, D. N. *Inorg. Chem.* **1976**, *15*, 607−618. (b) DeSimone, R. E. *J. Am. Chem. Soc.* **1973**, *95*, 6238−6244. (c) Heath, G. A.; Martin, R. L. *Aust. J. Chem.* **1970**, *23*, 1721−1734. (d) Webster, R. D.; Heath, G. A.; Bond, A. M. *Dalton Trans.* **2001**, 3189−3195.

4. Conclusion

Variable-temperature NMR spectral and electrochemical data of the $[HB(mt)_3]$ ligand at $Cp^*Ru^{II/III}$ have demonstrated a facile κ^3-S,S′,S″ and κ^3-H,S,S′ coordination exchange. The κ^3-S,S′,S″ and κ^3-H,S,S′ forms of both the Cp^*Ru^{II} and Cp^*Ru^{III} complexes are long enough lived in solution to be detected by cyclic voltammetry. The κ^3-S,S′,S″ form of $[Cp^*Ru^{III}\{HB(mt)_3\}]^+$ (**1A**) and the κ^3-H,S,S′ form of $[Cp^*Ru^{II}\{HB(mt)_3\}]$ (**2B**) are the preferred isomers in solution (although there is a strong temperature and solvent dependence), while in the solid state, the κ^3-S,S′,S″ forms are preferred for both Cp^*Ru^{III} (**1A**) and Cp^*Ru^{II} (**2A**).

A key factor that enabled quantification of the square scheme mechanism by cyclic voltammetry is that the rate constants for the conversions between the κ^3-S,S′,S″ and κ^3-H,S,S′ isomers were sufficiently low to permit only moderate voltammetric scan rates to be used ($v = 0.1-50$ V s^{-1}). Faster homogeneous rates require faster voltammetric scans and microelectrodes to avoid the effects of uncompensated solution resistance, which can complicate the data collection and interpretation in low-dielectric solvents such as CH_2Cl_2, especially when low temperatures are used. Conversely, very slow rates of homogeneous reaction are not detectable by cyclic voltammetry. Furthermore, the heterogeneous rates of electron transfer were sufficiently fast so as not to interfere with determination of the homogeneous rates of isomerization involving formation/breaking of the Ru−S bond.

Acknowledgment. We thank the National University of Singapore for Academic Research Fund Grant No. R143000209112 (L.Y.G.) and Ms. G. K. Tan for technical assistance. S.L.K. thanks Ms. M. Halim for preliminary assistance, and R.D.W. thanks the Australian Research Council for the award of a QEII Fellowship.

Supporting Information Available: X-ray crystallographic files in CIF format and crystallographic data and refinement details, for the structure determinations of **1A** and **2A** (Table S1), ^{1}H NMR spectral data of **2** in different solvent compositions of C_6D_6/CD_2Cl_2 and in CD_2Cl_2 at 183 K, Figures S1−S3 showing the 2D ^{1}H NMR COESY, NOESY, and EXSY spectra of **2A/2B** in C_6D_6, Figures S4 and S5 showing cyclic voltammograms and associated digital simulations of **1A** and **2A/2B**, and Figure S6 showing a voltammetric comparison of solutions of **1A** and ferrocene at several scan rates. This material is available free of charge via the Internet at http://pubs.acs.org.

OM050432O